J Mater Sci (2006) 41:5900–5906
DOI 10.1007/s10853-006-0268-4

The development of the microstructural and electrical characteristics of NTC thick-film thermistors during firing

Marko Hrovat · Darko Belavič · Janez Holc · Jena Cilenšek

Received: 21 April 2005 / Accepted: 11 October 2005 / Published online: 8 July 2006

Abstract One kohm/sq. thick-film NTC thermistors (4993, EMCA Remex) with high, non-linear and negative temperature coefficients of resistivity were fired at different temperatures. The development of the resistors' conductive phase and microstructure was investigated by X-ray diffraction analysis and by scanning electron microscopy. Sheet resistivities, beta factors and noise indices were measured as a function of the firing temperature. In the fired layers of the thermistors the X-ray analyses showed mainly spinel phase and RuO_2, which is added to the thick-film NTC materials to decrease the specific resistance and to improve the stability and the current noise. Higher firing temperatures led to more densely sintered microstructures, to increased resistivities and to higher beta factors. The higher resistivities were attributed to the partial exchange of ions on the ''*B*'' sites of the spinel structure with aluminium ions.

Introduction

The main requirements for thick-film resistors are long-term stability and relatively narrow tolerances of the sheet resistivities after firing. An important characteristic is a low temperature coefficient of resistivity (TCR), which for most modern resistors is around or under 50×0^{-6}/K. However, for some temperature-sensing applications resistors with a large temperature dependence of resistivity–thermistors—are required. The design flexibility, small size and lower cost of thick-film thermistors are advantageous when compared to discrete components.

Materials with large negative TCRs (NTC) are based on solid solutions of transition-metal oxides, in most cases, due to their long-term stability, Mn_3O_4, Co_3O_4 and NiO with the spinel structure (general formula AB_2O_4). The dependence of the specific resistance ρ versus temperature is described by:

$$\rho = \rho_0 \times \exp(B/T) \tag{1}$$

where ρ_0 (ohm m) is the resistivity at ''infinite'' temperature, T is the temperature (K) and B is the thermistor constant (K) (also called the beta factor or the coefficient of temperature sensitivity). Resistivity at ''infinite'' temperature is determined by the total number of ''*B*'' lattice sites that can take part in the ''hopping'' conductivity process (there is no contribution to the overall conductivity if ions with different valences are on the *A* sites because the distance between the two *A* sites in a spinel lattice is too great for an electron ''hopping'' mechanism). *B* is defined as the ratio between the activation energy for electrical conduction and the Boltzman constant. For the calculation of *B* from measured resistances at different temperatures equation (1) is normally written as

$$B = \ln(R_1/R_2)/(1/T_1 - 1/T_2) \tag{2}$$

where T is again the absolute temperature and R_1 and R_2 are the resistances at T_1 and T_2, respectively.

The values of the resistivities and the beta factors of NTC materials depend on the ratio of the oxides. The

M. Hrovat (✉) · J. Holc · J. Cilenšek
Jožef Stefan Institute, Jamova 39, SI-1000 Ljubljana, Slovenia
e-mail: marko.hrovat@ijs.si

D. Belavič
HIPOT-R&D, d.o.o., Trubarjeva 7, SI-8310 Sentjernej, Slovenia

resistivities range from a few hundred ohm cm to a few tens of kohm cm, the beta factors from 2500 K to 4000 K and the temperature coefficients of expansion from 8.5×10^{-6}/K to 14.3×10^{-6}/K [1–3]. A partial substitution of the iron oxide on the *B* sites or copper oxide on the *A* sites increases or decreases the resitivities, respectively [4–7].

After screen printing and firing the thick-film NTC thermistors basically consist of semi-conducting spinel and glass phases. The fired thickness is usually between 10 and 20 μm. As mentioned before, the resistivities of the different spinel compositions are between a few hundred ohm cm and a few tens of kohm cm, and can be increased up to 1 Mohm cm with the partial substitution of manganese or cobalt ions with iron ions. These are useful values for pellet-type components. However, due to the dimensions of the thick-film resistors the values of the sheet resistivities (ohm/sq.) are between two and three orders of magnitude higher than the resistivities (ohm cm) of the materials themselves. The glass phase, which is added for better sintering of the thick-film layers at relatively low firing temperatures (850 °C), further increases the resistivity. Therefore, materials for thick-film NTC resistors usually include some phase with a low specific resistance, generally RuO_2 which is a conductive phase, either in the form of ruthenium oxide or ruthenate, in most modern thick-film resistors. RuO_2 has a relatively low specific resistivity, 40×10^{-6} ohm cm, and a positive, linear, metallic-like dependence of resistivity versus temperature, with a TCR of 7000×10^{-6}/K for single crystals and a few 1000×10^{-6}/K for sintered microcrystalline samples [8, 9]. The addition of ruthenium oxide decreases the specific resistance, reduces the noise and improves the stability of the resistors [1, 10]. However, due to the high, positive TCRof the RuO_2 it also decreases the beta factors.

During firing, thick-film thermistors reach the highest temperature (850 °C) in 10 or 20 min., and are only a relatively short time (10 min,) at this temperature. During the firing cycle the constituents of the material react with each other. The reactions presumably do not reach equilibrium, so the characteristics of the fired materials are a consequence of this frozen non-equilibrium state.

In this paper the characterization of (a rather typical) 1 kohm/sq. thick-film NTC thermistor (4993, EMCA Remex) as a function of firing temperature will be described and discussed. The aim of the work is to gain some insight into the development of the thick-film thermistor's electrical characteristics, i.e., sheet resistivity, beta factor and noise, and microstructural characteristics, during the firing process. Thermistors were fired at temperatures from 500 °C to 950 °C, and also for a relatively long time (3 h) at 950 °C to allow reactions to reach or at least to come close to equilibrium.

Experimental

Thick-film thermistors were printed on 96% alumina substrates, dried for 15 min at 150 °C and fired for10 min at temperatures from 500 °C to 950 °C, and for 3 h at 950 °C. The resistors were terminated with a Pd/Ag conductor that was prefired at 850 °C. The electrical characteristics (sheet resistivity, resistivity versus temperature and noise) were measured on resistors with dimensions of 1×1 mm^2. Cold TCRs (from –25 °C to 25 °C) and hot TCRs (from 25 °C to 125 °C) were calculated from resistivity measurements at –25 °C, 25 °C, and 125 °C. The current noise was measured in dB on 100-mW loaded resistors using the Quan Tech method—MIL-STD-202B, Method 308—(Quan Tech Model 315-C). The resistors were also evaluated using complex-impedance analysis (Hewlett Packard 4192-A, 5 Hz to 13 MHz).

The dimensions of the resistors for the microstructural analyses and the X-ray diffraction analyses, which were printed and fired without conductor terminations, were 8×8 mm^2. The dried resistors and the resistors fired at different temperatures were examined by X-ray powder-diffraction (XRD) analysis with a Philips PW 1710 X-ray diffractometer using Cu K_α radiation. The X-ray diffraction spectra were measured from $2\ \Theta = 20^o$ to $2\ \Theta = 70°$ in steps of 0.02°. For the microstructural investigation the resistors, which were printed and fired on alumina ceramics, were mounted in epoxy in a cross-sectional orientation and then cut and polished using standard metallographic techniques. A JEOL JSM 5800 scanning electron microscope (SEM) equipped with a LINK ISIS 300 energy-dispersive X-ray analyser (EDS) was used for the microstructural and compositional analysis. Prior to analysis in the SEM, the samples were coated with carbon to provide electrical conductivity and to avoid charging effects. Boron oxide, which is also present in the glass phase, cannot be detected in the EDS spectra because of the low relative boron weight fraction in the glass and the strong absorption of the boron Kα line during EDS analysis in the glass matrix.

Results and discussion

The X-ray diffraction spectra of the 4993 thermistors that were dried at 150 °C and fired at different temperatures are shown in—the rather over-crowded—Fig. 1. The spectrum of RuO_2, denoted ''RuO2'', is also included in the graph. The peaks of spinel phase ($(Ni,Cu)(Co,Mn)O_4$), see EDS analysis in the Table 1, are denoted ''SP''. The spectra of the dried thermistors and of the thermistors fired at 500 °C are similar. The peaks of the spinel phase are not present. After firing at 700 °C the peaks of the spinel phase start to

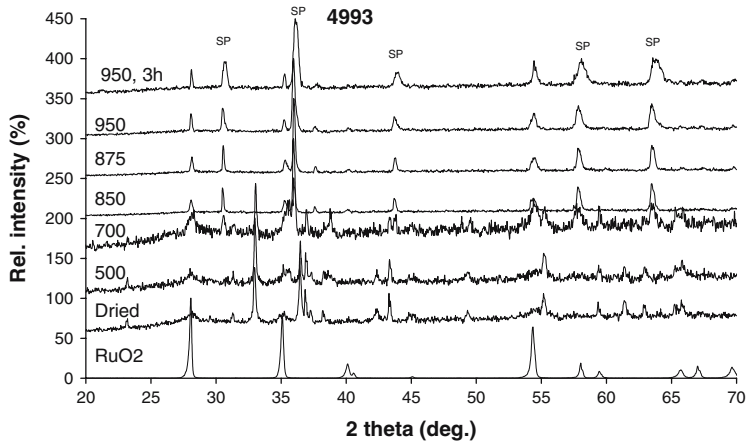

Fig. 1 X-ray diffraction spectra of the NTC 4993 thermistors dried at 150 °C and fired at different temperatures. The spectrum of ruthenate, denoted ''RuO2'', is also included. The peaks of spinel phase are denoted ''SP''

appear, while the original peaks of the dried material are still present. After firing at 850 °C, as well as at higher temperatures mainly the peaks of the spinel phase and of the ruthenium oxide are observed. It is interesting to note that the semi-conducting spinel phase is not present in the un-fired thermistor but forms during firing. The temperature of the synthesis of the spinel solid solution is relatively low as its peaks are present in the XRD spectra already after firing for just 10 minutes at 700 °C, while in the production of discrete components the required firing temperatures are from 1000 °C to over 1200 °C [4, 11, 12]. The lower temperature of spinel synthesis in thick-films as compared to bulk ceramics is presumably due to the presence of a liquid glass phase which in thick-film resistors appears at temperatures around 700 °C [13, 14].

The microstructures of the surfaces of the NTC 4993 thermistors dried at 150 °C, and then fired for 10 min at 850 °C and 3 h at 950 °C are shown in Figs. 2a, b and c, respectively. The dried paste is a mixture of lighter grains (glass phase) and darker grains. The light grains are composed mainly of SiO_2 and PbO with around 5 mol% of alumina. The EDS analysis of the darker phase shows the presence of Mn, Co, Ni, Cu and Ru oxides. The microstructure of the surface of the thick-film thermistors fired at 850 °C is glassy and porous with pore dimensions up to 10 μm. The surface of the thermistors fired for 3 h at 950 °C is similar, but less porous.

The microstructures of cross-sections of thick-film thermistors fired at different temperatures are shown in Fig. 3a (850 °C), b (875 °C), c (950 °C) and d (950 °C, 3 h). In all the pictures the alumina substrate is on the right. After firing for 10 min at 850 °C and 875 °C the layer is rather porous, while after firing for 10 min and 3 h at 950 °C it is densely sintered. The overall analysis of the layer (area 15×15 μm^2) showed the presence of mainly Al, Si, Mn, Co, Ni, Cu, Ru and Pb. As mentioned in the Introduction, the copper oxide is added to lower the specific resistance of the Mn–Co–Ni solid solution. The results of analysis are present in Table 1. The compositions are given in atomic and weight percent. The concentration of oxygen is calculated by difference and not measured directly. The elemental ratio between Mn–, Co– and Ni–oxides is roughly 5/2/1, which puts this composition in the region of solid solutions with the lowest specific resistances between 0.5 and 1 kohm cm [3]. Some other oxides with concentrations below 1 at. % (MgO, K_2O and CaO), which are also detected, are not included in Table 1.

The light coloured phase in all the samples is a glass phase, rich in silica, alumina and lead oxide. The darker phase is rich on manganese, cobalt, nickel, copper and ruthenium oxide, and is presumably a mixture of Mn–Co–Ni–Cu–O solid solution and RuO_2. The thin (around 1 μm) layer on the interface between the thermistor film and the alumina substrate is composed mainly from alumina, silica and lead oxide. The concentration of Al_2O_3 is roughly two times higher than in the glass in the thermistor and originates from the substrate. This liquid penetrates into the substrate promoting the growth of Al_2O_3 grains, presumably due to the dissolution–precipitation mechanism. The depth of penetration increases with increasing firing temperature and time. It varies from around 5 μm after firing at 850 °C to over 20 μm after firing at 950 °C for 3 h. After 3 h firing at 950 °C a relatively thick (around 5 μm, i.e. one third of thermistor thickness) dark glassy layer between the thermistor film and the substrate is observed. EDS analysis of the dark layer shows a very high concentration, around 45 wt. %, of alumina. Other oxides present are Mn–, Co–, Ni– and Cu oxides. The concentrations of silica and lead oxide are only a few tenths of percent. The overall concentration of alumina in thermistors fired for 3 h at 950 °C is 24 wt. %, which is significantly higher than the concentration in thermistors fired for 10 min at 950 °C (17 wt. %).

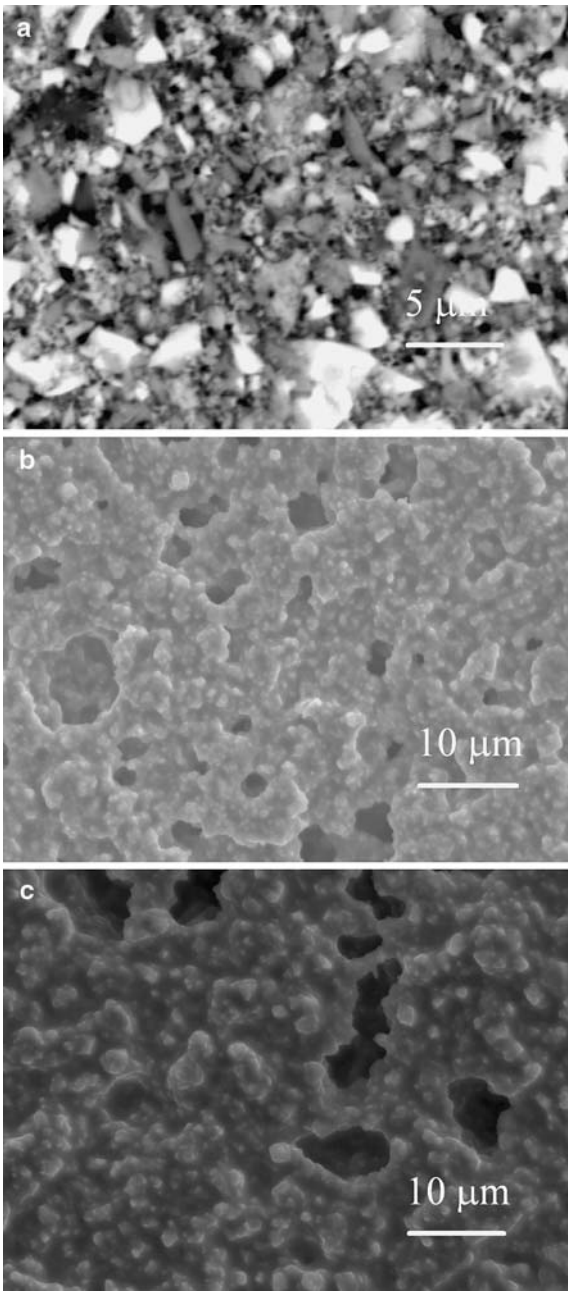

Fig. 2 (a) The microstructure of the surface of the NTC 4994 thermistor dried at 150 °C. Back-scattered electrons, (b) The microstructure of the surface of the NTC 4994 thermistor fired 10 min at 850 °C. Secondary electrons, (c) The microstructure of the surface of the NTC 4994 thermistor fired 3 h at 950 °C. Secondary electrons

The sheet resistivities, cold (–25 °C to 25 °C) and hot (25 °C to 125 °C) TCRs, the beta factors and the noise indices of the NTC 4993 thick-film thermistors, fired for 10 min at temperatures from 700 °C to 950 °C and for 3 h at 950 °C, are shown in Table 2. The sheet resistivities and therefore all the other electrical characteristics of the 4993 thermistors fired below 700 °C are too high to measure. The dependence of the logarithm of sheet resistivity versus firing temperature, the logarithm of resistivity versus temperature, and of the noise indices versus firing temperature are graphically presented in Figs. 4, 5 and 6, respectively. Note that in Fig. 6 the noise indices are expressed in ''uV/V'' while in Table 2 they are given as ''dB''.

The sheet resitivities of the NTC thermistors fired below 700 °C are too high t be measured. After firing at 700 °C the sheet resistivities of the thick-film 4993 thermistors (see also Fig. 4) are rather high, around 75 kohm/sq. At higher firing temperatures, up to 900 °C, they decrease to a nominal sheet resitivity. At even higher firing temperatures the resistivities increase again. After 3 h firing at 950 °C they reach 27 kohm/sq. A measurable resistivity appears after firing at 700 °C when the spinel phase starts to form, as shown in the XRD spectra in Fig. 1. The high sheet resisitivities of samplesafter firing for 3 h at 950 °C are presumably due to the partial substitution of *B* site ions with Al^{3+} ions in the spinel structures with the empirical formula $A^{2+}(x\mathrm{Ni}^{2+}x\mathrm{B}^{4+}(2–x–y)\mathrm{B}^{3+}y\mathrm{Al}^{3+})\mathrm{O}_4$ (*B*–Mn or Co). The incorporated aluminium ions in the *B* sites decrease the content of manganese and cobalt ions. This decrease leads to a reduction of the number of ions that are capable of either donating or accepting electrons (for example, Mn^{3+} and Mn^{4+}, respectively) resulting in an increase of the resistivity [5]. This supposition is tentatively confirmed by the XRD analysis. The peaks of spinel phase in the NTC thermistors fired for 3 h at 950 °C are broad and shifted to lower *d*-values. Presumably, the decrease of the unit-cell dimensions is due to the smaller ionic radius of Al^{3+} (Al^{3+} CN 6 0.535 nm) compared with the radii of Mn^{3+} (Mn^{3+} CN6 0.58 nm) or Co^{3+} (Co^{3+}CN 6 0.55 nm) [15]. Broad peaks of the spinel phase are due to non homogenous solid solutions.

The beta factors decrease with increasing firing temperature from 700 °C to 900 °C, from around 2000 K to 1150 K, and then increase to over 1800 K for samples fired for 3 h at 950 °C. The resistivity versus temperature measurements are shown in Fig. 6. Due to similar sheet resistivities and beta factors the resistivity versus temperature curves for the samples fired for 10 min at 850 °C and 875 °C, and at 800 °C and 950 °C, nearly overlap.

The noise indices of the 4993 thermistors are relatively low, regardless of the firing conditions and can be compared with the noise indices of the ''ordinary'' thick-film resistors with low TCRs and with the same nominal sheet resistivities, i.e, 1 kohm/sq., which are around –18 dB (0.1 to 0.2 uV/V) [16].

The complex-impedance plot of the 4399 thermistors fired at different temperatures is shown in Fig. 7.a. An enlarged inset from Fig. 7.a is shown in Fig. 7.b. The real

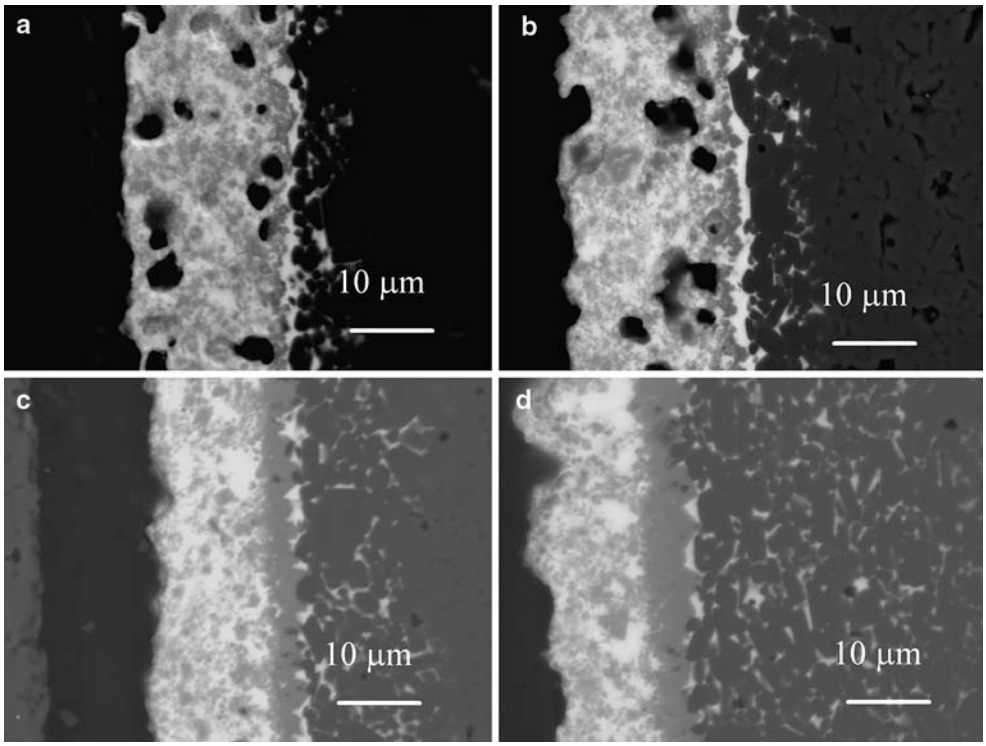

Fig. 3 (a) The microstructure of cross-section of 4993 NTC thermistor fired 10 min at 850 °C. The alumina substrate is on the right. Back-scattered electrons, (b) The microstructure of cross-section of 4993 NTC thermistor fired 10 min at 875 °C. The alumina substrate is on the right. Back-scattered electrons, (c) The microstructure of cross-section of 4993 NTC thermistor fired 10 min at 950 °C. The alumina substrate is on the right. Back-scattered electrons, (d) The microstructure of cross-section of 4993 NTC thermistor fired for 3 h at 950 °C. The alumina substrate is on the right. Back-scattered electrons

Table 1 The EDS analyses of the concentration of elements in atomic % and weight % over the 15×15 μm^2 area of the cross-sections of the NTC films

Element	at. %	Oxide	wt. %
Al	7.1	Al_2O_3	9.7
Si	5.8	SiO_2	9.4
Mn	10.4	MnO	21.6
Co	4.0	CoO	8.0
Ni	2.2	NiO	4.5
Cu	7.3	CuO	15.4
Ru	2.3	RuO_2	7.8
Pb	3.8	PbO	22.5
O	56.2		

Table 2 Sheet resistivities, cold (–25 °C to 25 °C) and hot (25 °C to 125 °C) TCRs, beta factors and noise indices of the NTC 4993 thermistors

T firing (°C)	R sheet (kohm/sq.)	Cold TCR ($\times 10^{-6}$/K)	Hot TCR ($\times 10^{-6}$/K)	*B*(K)	Noise (dB)
700	75	–47180	–8030	1910	–10.7
750	5.7	–57500	–8260	2030	–21.4
800	1.5	–42490	–7640	1700	–17.0
850	0.55	–22930	–6530	1240	–12.9
875	0.55	–20870	6180	1150	–21.6
900	0.72	–21080	–6260	1160	–17.6
950	1.5	–26550	–6770	1340	–20.4
950, 3 h	27	–47470	–7820	1820	–16.1

part –R– is a function of the resistivity changes while the imaginary part –X– is an indication of the dielectric characteristics. After firing between 800 and 900 °C the thermistors show a nearly ideal resistor response, presumably due to the complete formation of a semiconductive spinel phase at 800 °C, as seen from the X-ray spectra (Fig. 1). However, at lower and higher firing temperatures the resistors have a relatively large imaginary part, which can be explained as a parallel combination of resistors and capacitors with the plot maximum at $\omega RC = 1$. The imaginary part for the thermistors fired at temperatures lower than 800 °C is presumably due the incomplete formation of the semiconductive spinel phase, which is partially separated by the glass phase. High values of the real and imaginary parts of the impedance after firing at 950 °C for 3 h could be tentatively explained by the above-mentioned incorporation of aluminium ions in the spinel phase ($Ni_{1-x}(Ni_xMn_{1-y}Co_y)_2O_4$) and the resulting increase of the resistivity.

Conclusions

Thick-film NTC thermistors (4993, EMCA Remex, 1 kohm/sq. nominal resitivity) were fired at different temperatures. The dried thermistors and the thermistors fired at different temperatures were examined by XRD, SEM, and EDS microanalysis to determine the influence of firing temperature on the electrical and microstructural characteristics.

The semiconductive spinel phase is not present in the dried thermistors but is formed during firing. After firing at 700 °C the sheet resistivities of thick-film thermistors are rather high, at higher firing temperatures, up to 900 °C,

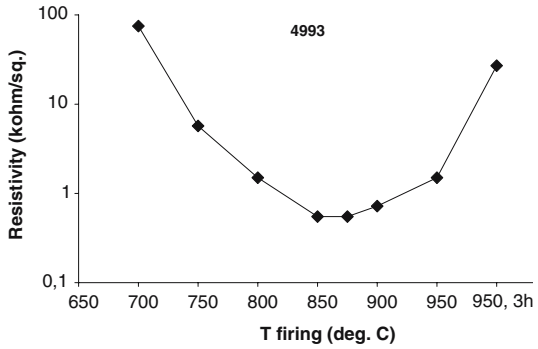

Fig. 4 Logarithm of sheet resistivity versus firing temperature for NTC 4994 thermistors

they decrease to a nominal sheet resitivity. At even higher firing temperatures the resistivities increase again. The beta factors decrease with increasing firing temperature and than increase to over 1800 K for samples fired at higher temperatures. The noise indices are relatively low, regardless of the firing conditions.

After firing at 850 °C and at higher temperatures, mainly the spinel phase and the ruthenium oxide are observed in XRD spectra. EDS analyses showed that the ratio between the Mn–, Co– and Ni–oxides is roughly 5/2/1, which puts this composition in the region of $Ni_{1-x}(Ni_xMn_{1-y}Co_y)_2O_4$ solid solutions with the lowest specific resistances. Due to interactions between the glass phase in the thermistor film and the alumina substrate, the overall concentration of alumina in the thermistor layer after 3 h at 950 °C increases significantly. The high sheet resisitivities of samples fired for 3 h at 950 °C are presumably due to partial substitution of the *B* site ions with Al^{3+} ions in the spinel structures.

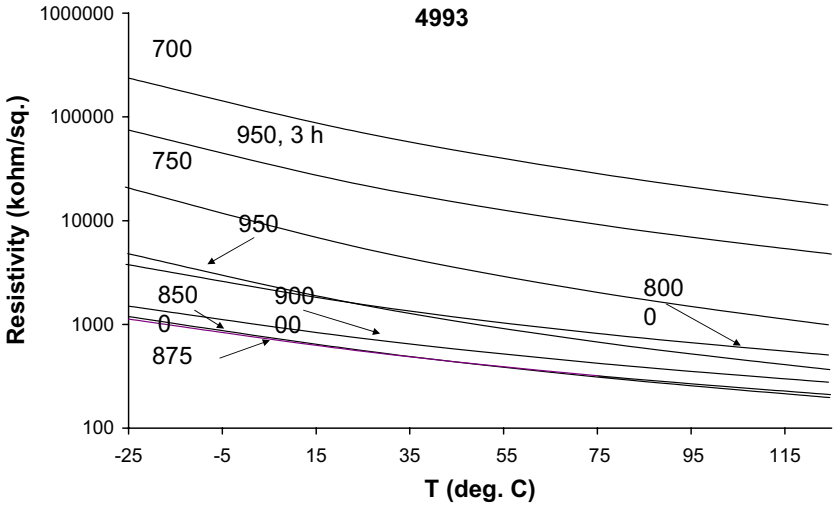

Fig. 5 Logarithm of sheet resistivity versus temperature for NTC 4994 thermistors, fired at different temperatures

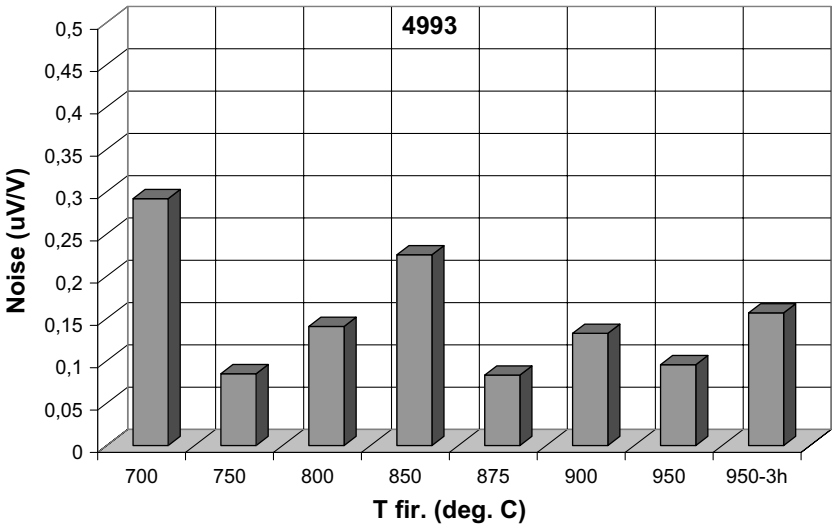

Fig. 6 The dependence of noise indices versus firing temperature for NTC 4994 thermistors

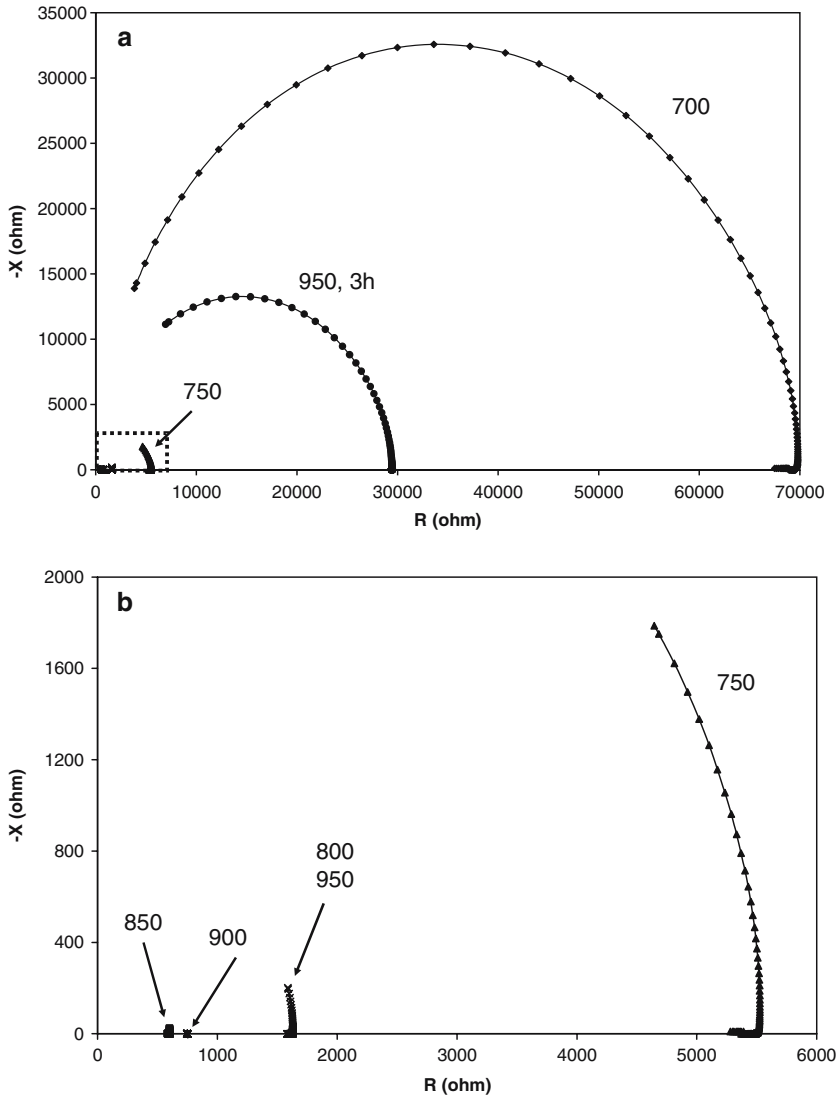

Fig. 7 (a) The complex-impedance plot of the NTC 4994 thermistors, fired at different temperatures. The real part -R- is a function of resistivity changes while the imaginary part -X- is an indication of the dielectric characteristics, (b) Inset from Fig. 7(a)—the complex-impedance plot of the NTC 4994 thermistors, fired at temperatures from 750 °C to 950 °C

Acknowledgements The authors wish to thank Mr. Mitja Jerlah (HIPOT-HYB) for printing and firing the samples as well as for measuring the electrical characteristics. The financial support of the Slovenian Research Agency is gratefully acknowledged.

References

1. Martin de Vidales JL, Garcia-Chain P, Rojas RM, Vila E, Garcia Martinez O (1998) J Mater Sci 33(6):1491
2. Huang J, Hao Y, Lin H, Zhang D, Song J, Zhou D (2003) Mater Sci Eng B99(1–3):523
3. M-Prudenziati (ed) (1994) Thick film sensors. Elsevier, Amsterdam, pp 127–150
4. Martinez Sarrion ML, Morales M (1995) J Mater Sci 30(10):2610
5. Park K, Bang DJ (2003) J Mater Sci: Materials in Electronics 14:81
6. Metz D, Caffin P, Legros R, Rousset A (1989) J Mater Sci 24(1): 83
7. Metz R (2000) J Mater Sci 35(18):4705
8. van Loan PR (1972) Ceram Bull 51(3):231, 242
9. Pierce JW, Kuty DW, Larry JR (1982) Solid State Technol 25(10):85
10. Hao YD, Chen LJ, Lin H, Zhou DX, Gong SP (1993) Sensors Actuators A35(3):269
11. Macklen ED (ed) (1979) Thermistors, Electrochemical Publications Ltd., Ayr, pp 16–28
12. Park K (2004) Scripta Materialia 50:551
13. Hrovat M, Jan F (1987) Hybrid Circuits 14:25
14. Hrovat M, Samardžija Z, Holc J, Belavič D (2002) J Mater Sci 37:2331
15. Shannon RD (1976) Acta Cryst A32:751
16. Hrovat M, Benčan A, Belavič D, Holc J, Dražič G (2003) Sensors and Actuators A103:341